Laser Heating of Metallic Surfaces

Massachusetts Inst. of Tech.

May 20, 1976

Project Report

LTP-31

Laser Heating of Metallic Surfaces

S. Marcus
J. F. Lowder
S. K. Manlief
D. L. Mooney

20 May 1976

Prepared for the Defense Advanced Research Projects Agency under Electronic Systems Division Contract F19628-76-C-0002 by

Lincoln Laboratory
MASSACHUSETTS INSTITUTE OF TECHNOLOGY
LEXINGTON, MASSACHUSETTS

The work reported in this document was performed at Lincoln Laboratory, a center for research operated by Massachusetts Institute of Technology. This work was sponsored by the Defense Advanced Research Projects Agency under Air Force Contract F19628-76-C-0002 (ARPA Order 600).

This report may be reproduced to satisfy needs of U.S. Government agencies.

This technical report has been reviewed and is approved for publication.

FOR THE COMMANDER

William H. Lawton

William H. Lawton, Lt. Col., USAF
Acting Chief, ESD Lincoln Laboratory Project Office

UNCLASSIFIED

SECURITY CLASSIFICATION OF THIS PAGE *(When Data Entered)*

REPORT DOCUMENTATION PAGE

READ INSTRUCTIONS BEFORE COMPLETING FORM

1. REPORT NUMBER: ESD-TR-76-122	2. GOVT ACCESSION NO.
3. RECIPIENT'S CATALOG NUMBER	
4. TITLE *(and Subtitle)*: Laser Heating of Metallic Surfaces	5. TYPE OF REPORT & PERIOD COVERED: Project Report
6. PERFORMING ORG. REPORT NUMBER: Project Report LTP-31	
7. AUTHOR(s): Stephen Marcus, Scott K. Manlief, J. Elbert Lowder, Daniel L. Mooney	8. CONTRACT OR GRANT NUMBER(s): F19628-76-C-0002
9. PERFORMING ORGANIZATION NAME AND ADDRESS: Lincoln Laboratory, M.I.T., P.O. Box 73, Lexington, MA 02173	10. PROGRAM ELEMENT, PROJECT, TASK AREA & WORK UNIT NUMBERS: ARPA Order 600, Program Element No. 62301E, Project No. 6E20
11. CONTROLLING OFFICE NAME AND ADDRESS: Defense Advanced Research Projects Agency, 1400 Wilson Boulevard, Arlington, VA 22209	12. REPORT DATE: 20 May 1976
	13. NUMBER OF PAGES: 44
14. MONITORING AGENCY NAME & ADDRESS *(if different from Controlling Office)*: Electronic Systems Division, Hanscom AFB, Bedford, MA 01731	15. SECURITY CLASS. *(of this report)*: Unclassified
	15a. DECLASSIFICATION DOWNGRADING SCHEDULE

16. DISTRIBUTION STATEMENT *(of this Report)*

Approved for public release; distribution unlimited.

17. DISTRIBUTION STATEMENT *(of the abstract entered in Block 20, if different from Report)*

18. SUPPLEMENTARY NOTES

None

19. KEY WORDS *(Continue on reverse side if necessary and identify by block number)*

thermal coupling
laser heating
calorimetric techniques
metallic surfaces

20. ABSTRACT *(Continue on reverse side if necessary and identify by block number)*

Enhanced thermal coupling of pulsed 10.6 μm laser radiation to aluminum, copper, and titanium targets has been investigated as a function of incident fluence, focal spot size, and ambient pressure, using both calorimetric and fast-response surface-thermocouple techniques. The fraction of energy coupled to the target within the focal spot was found to increase with increasing spot size. Under conditions of low ambient pressure (≈ 0.05 torr), the thermal coupling for aluminum at high incident fluences was roughly a factor of 2 higher than at atmospheric pressure.

DD FORM 1 JAN 73 1473 EDITION OF 1 NOV 65 IS OBSOLETE

UNCLASSIFIED

SECURITY CLASSIFICATION OF THIS PAGE *(When Data Entered)*

MASSACHUSETTS INSTITUTE OF TECHNOLOGY

LINCOLN LABORATORY

LASER HEATING OF METALLIC SURFACES

S MARCUS

Group 53

J E LOWDER
S K MANLIEF

Group 51

D. L. MOONEY

Aeronutronic Ford Corporation

PROJECT REPORT LTP-31

20 MAY 1976

ABSTRACT

Thermal coupling of pulsed 10.6 μm laser radiation to aluminum, copper, and titanium targets has been measured as a function of incident fluence focal spot size, and ambient pressure, using both calorimetric and fast-response surface-thermocouple techniques. A peak enhancement in thermal coupling of approximately a factor of ten was observed to occur at the onset of a well-developed plasma at the surfaces of the copper and aluminum targets. After passing through a maximum, the enhanced coupling decreased with increasing fluence and approached CW values at high incident laser fluences. For small spot sizes (area $\lesssim 0.03$ cm^2), most of the enhanced absorption occurred outside the focal spot. The fraction of energy coupled to the target within the focal spot increased with increasing spot size. Under conditions of low ambient pressure (~ 0.5 torr), the breakdown threshold was increased by a factor of 5, and at high incident fluences the thermal coupling for aluminum was roughly a factor of 2 higher than at atmospheric pressure.

CONTENTS

LASER HEATING OF METALLIC SURFACES

I. INTRODUCTION

Recent thermal coupling measurements[1-3] have shown that if the incident laser intensity is sufficient to cause a breakdown at a surface, the thermal coupling coefficient can differ markedly from its low intensity value. Specifically, for normally highly reflecting metals such as aluminum, enhancement of an order of magnitude or more was observed. This enhancement is due to the high absorptivity of the generated plasma and subsequent energy transfer to the surface. The referenced measurements were done with small spots, and one might expect the radial expansion of the plasma to cause much of the energy to be deposited well outside of the focal spot. The degree to which the plasma is contained within the focal spot is of importance since it is the coupled laser fluence which is effective in reducing the time required for target burn-through. In order to investigate the spatial and temporal characteristics of the enhanced coupling, a series of small spot measurements were performed using front-surface-thermocoupled targets and are discussed in Section II. These results are then compared to large-spot measurements which are discussed in Section III.

II. SMALL-SPOT EXPERIMENTS

For the small-spot coupling a target of the type shown in Figure 1 was constructed. The thermocouples, manufactured by Medtherm, Inc., are fabricated by swaging a chromel tube over an aluminum oxide-coated alumel wire of 1 to 10 mil diameter. The thermocouple assembly is then inserted into a

drilled metal slab and polished flush with the surface. The thermocouple junction is completed by vapor depositing a 1 - 2 μm layer of the metal whose absorptivity is to be measured. Using thermocouples thus constructed, one can obtain surface temperature measurements with microsecond time response and 10 mil spatial resolution.

Figure 2 shows schematically the experimental layout for our thermal coupling measurements. Initial experiments were performed with a small electron-beam CO_2 laser from which were obtained single, rectangular in time, 5-joule pulses of ≈ 20 μsec duration. The pulse shape and energy were monitored by reflections from a KCl wedge by photon drag and $BaTiO_3$ detectors. After passing through the wedge, the beam was focussed to a 2 mm spot onto the target surface where the presence of plasma was detected by a photomultiplier.

Figure 3 shows a typical temperature history of a copper surface when no plasma is observed. The open circles are digitized data points, and the solid curve is a theoretical fit which is discussed below. Note that without plasma, the surface temperature stops its increase abruptly at the end of the pulse, and then decreases as heat is conducted into the bulk material.

Such is not the case when breakdown occurs on the surface, as is shown in Figure 4. In this case, the temperature peaks well before the end of the pulse, and there is no abrupt change in the curve at t_p. To extract coupling information from these temperature responses, it is necessary to relate them to the surface heating rate. The theory for this inversion is developed in the next section.

A. Theoretical Development

Thermal response to an incident pulse depends markedly on the thermocouple junction depth below the surface. As the junction depth is increased, the diffusion of heat laterally in the surface layer becomes important. A computer code has been generated to solve the time-dependent heat-flow equation in the case of axial symmetry about the thermocouple. For thermocouples with surface layers less than 1 μm thick, the results indicate that an infinite copper-constantan thermocouple (i.e., a thin copper layer over a semi-infinite constantan slab) is a reasonable model. (For specificity, copper-constantan thermocouples are considered in this discussion - the theory applies equally to other materials.)

1. Surface Thermocouples

A thermocouple with a copper surface layer thickness less than 1 μm can be analyzed by assuming that the thermal properties are essentially those of a semi-infinite block of constantan. For such a case, the temperature change T and the absorbed flux F are related by the following equations[4]

$$T(0,t) = \sqrt{\frac{k}{\pi}}\,\frac{1}{K}\int_0^t \frac{F(0,t')\,dt'}{\sqrt{t-t'}}$$

$$F(0,t) = \frac{K}{\sqrt{\pi k}}\int_0^t \frac{\frac{d}{dt'}\,T(0,t')\,dt'}{\sqrt{t-t'}}\,, \qquad (1)$$

where the thermal properties are those of constantan.

The most straightforward procedure is to use Equation (1) and expand T in some basis set. A linear spline expansion is used nere

$$T(0,t) = \Sigma\, T_i W_i(t) \quad .$$

Here the spline function is defined by

$$W_i(t) = \begin{cases} \dfrac{t - t_{i-1}}{t_i - t_{i-1}} & t_{i-1} < t < t_i \\ \dfrac{t_{i+1} - t}{t_{i+1} - t_i} & t_i < t < t_{i+t} \end{cases} \quad .$$

The resulting finite difference equations are given by

$$F_j = \frac{K}{\sqrt{k\pi}} \sum_{i=2}^{j} \frac{T_i - T_{i-1}}{t_i - t_{i-1}} \, 2\left(\sqrt{t_j - t_i} - \sqrt{t_j - t_{i-1}}\right) \quad ,$$

$$T_i = \sqrt{\frac{k}{\pi}} \, \frac{1}{K} \sum_{j=2}^{i} \frac{F_j - F_{j-1}}{t_j - t_{j-1}} \, \frac{2}{3} \left[2(t_i - t_{j-1})\sqrt{t_i - t_{j-1}} - 2(t_i - t_j)\sqrt{t_i - t_j}\right] \qquad (2)$$

These equations have been used with limited success to determine F. The basic problem with this approach is the numerical derivative. By integrating Equation (2) by parts, an alternative starting point is given by

$$F(0,t) = \frac{K}{\sqrt{\pi k}} \left[\frac{T(0,t)}{\sqrt{t}} + \frac{1}{2} \int_o^t \frac{T(0,t) - T(0,t')}{(t - t')^{3/2}} \right] .$$

The numerical derivative is still present implicitly in the second term, however, and the numerical procedure still amplifies small random errors incurred by digitizing the experimental temperature points T_i. This is a general problem for inversions where the integrand is generated by experimental data. A root-mean-square fit to the temperature also can be used. Because of the presence of a cusp in the thermocouple response, a fit in the range $t < t_p$ and a second in the range $t > t_p$ are the most reasonable choices. A second alternative is to expand the pulse in a polynomial expansion in the same way and adjust the coefficients with a rms fit of the experimental temperature points.

2. Polynomial Approximation of F(t)

From the previous section there are two equations which can be used to determine the absorbed flux. Because of the difficulties associated with numerical derivatives of the temperature, the equation which defines the junction temperature in terms of the surface flux will be the starting point. The flux will be expanded in a polynomial over two ranges; the first from zero to the time associated with the peak temperature and the second from the peak to the maximum time recorded.

$$F(t) = \begin{cases} \Sigma C_n t^n & 0 < t < t_p \\ \Sigma C'_n t^n & t_p < t < t_m \end{cases} .$$

For times less than t_p the temperature is given by

$$T = \sqrt{\frac{k}{\pi}} \frac{1}{K} \Sigma C_n \int_o^t \frac{t'^n dt'}{\sqrt{t - t'}}$$

$$= \Sigma C_n L_n (t) .$$

The evaluation of the integrals is accomplished by an 8th-order Gauss-Jacobi quadrature.

$$\int_o^t \frac{g(x)}{x^{1/2}} dx = \sum_{i=1}^{8} f(x_i) W_i$$

This procedure will integrate a 15th-order polynomial exactly and the values of x_i and W_i are given in Reference 5.

The root-mean-square fit of the temperature is given by minimizing the variation of the mean-square deviation as follows

$$\frac{\delta}{\delta C_n} \sum_1^N [T_i - T(t_i)]^2 = 0,$$

where T_i is the temperature at time t_i obtained by digitizing the recorded temperature histories and N is the number of measurements made before the end of the pulse.

For most reasonable pulses with a thin surface layer, a 4th-order polynomial is sufficient to describe F(t). For thicker layers, higher-order integration schemes are needed to take into account the rapid change in $K\beta/(t - t')$ at $t \to t'$.

For times greater than t_p, the temperature contribution due to flux absorbed before t_p is given by

$$T^*(t) = \sqrt{\frac{k}{\pi}} \frac{1}{K} \sum C_n \int_{t_p}^{t} \frac{t'^n}{(t - t')^{1/2}} \quad .$$

If there is flux absorption after t_p, this term is only a partial contribution to the temperature. The remaining part or residual temperature increase is given by

$$\Delta T(t) = \sqrt{\frac{k}{\pi}} \frac{1}{K} \int_{t_p}^{t} \sum \frac{C_n' \, t'^n dt'}{\sqrt{t - t'}}$$

$$\equiv \sum C_n' \, L_n'(t) \quad .$$

This situation is illustrated in Fig. 5. The values of C_n' are determined by the same procedure used to determine the values of C_n.

3. Arbitrary Junction Depth

For a semi-infinite thermocouple composed of a layer of copper of thickness ℓ and a semi-infinite constantan substrate, the time dependence of the temperature in the solid due to an arbitrary absorbed flux $F(-\ell, t)$ is governed by the following equations.

$$\frac{\delta^2 T}{\delta z^2} - \frac{1}{k'} \frac{\delta T}{\delta t} = 0 \qquad -\ell < z \leq 0$$

$$\frac{\delta^2 T}{\delta z^2} - \frac{1}{k} \frac{\delta T}{\delta t} = 0 \qquad 0 < z \quad .$$

The coordinate system is illustrated in Fig. 6. The boundary conditions are as follows.

$$K' \left.\frac{\delta T}{\delta z}\right|_{-\ell} = F(-\ell, t)$$

$$K' \left.\frac{\delta T}{\delta z}\right|_{-0} = K \left.\frac{\delta T}{\delta z}\right|_{+0}$$

$$T(\to \infty) = 0 \quad .$$

Here K and k are the thermal conductivity and thermal diffusivity of the substrate. A similar definition applies to the primed values for the surface layer.

The Laplace transform of T is designated by ν, and at the junction (i.e., $z = 0$) the value of ν is determined by the usual procedure of matching boundary conditions.[6] Since only the temperature at $z = 0$ and the absorbed flux at $x = -\ell$ are of interest in the following discussion, the z dependence will be implicitly understood. The resulting expression for ν is given by

$$\nu(s) = f(s)\,[Kq \cosh(q'\ell) + K'q' \sinh(q'\ell)]^{-1} \quad .$$

Here $q = \sqrt{s/k}$, similarly for q', and f(s) is the Laplace transform of the absorbed flux. This may be rearranged by expanding the hyperbolic functions

$$\nu(s) = 2f(s)\sqrt{\frac{k}{sK^2}}\,\frac{1}{1+\sigma}\sum_{n=0}^{\infty}\alpha^n e^{-(2n+1)\ell q'} \quad .$$

Here $\sigma = (K/K')\sqrt{k'/k}$ and $\alpha = (\sigma - 1)/(\sigma + 1)$.

The temperature at the junction is given by the inverse Laplace transform of $\nu(s)$

$$T(t) = \sqrt{\frac{k}{\pi}}\,\frac{1}{K}\int_0^t \frac{F(t')}{(t-t')^{1/2}}\,R[\ell^2/4k'(t-t')]\,dt',$$

where

$$R(y) = (1-\alpha)\sum_{n=0}^{\infty}\alpha^n e^{-(2n+1)^2 y} \quad .$$

A plot of R is shown in Fig. 7.

For completeness, the absorbed flux as a function of junction temperature is also given by

$$F(t) = K\sqrt{\frac{1}{\pi k}}\int_0^t \frac{dT(t')}{dt'}\,\frac{e^{b/(t-t')}dt'}{(t-t')^{1/2}} \quad ,$$

where $b = \ell^2/4k'$.

B. Single Thermocouple

Using the results of the previous sections, the instantaneous surface heating rate of our copper-coated target was obtained and is shown in Figure 8. This figure shows the case where the laser intensity was insufficient to cause breakdown. We see that, as one might expect, there is a sharp cutoff of energy absorption with the end of the laser pulse. The finite tail is taken to be a measure of the error in the inversion procedure.

In the case shown in Figure 9, the gain-switched spike initiated a breakdown on the target surface. The heating rate rises sharply early in the pulse as the plasma becomes opaque, but then peaks and declines as the plasma propagates and decouples the laser radiation from the target. Note, however, that there is significant heating after the laser pulse due to energy transfer from the residual plasma.

The curves of Figure 10 show the time-varying surface absorption coefficient for the cases discussed above as well as for an intermediate case. The absorption coefficients were obtained by inverting the temperature time-histories to determine the absorbed intensity and then dividing by the incident laser intensity. We see that there is roughly a two-fold enhancement in the focal spot coupling with a well-defined breakdown. This is much less than the order of magnitude enhancement previously reported.

C. Thermocouple Array

To test our hypothesis that this is due to energy deposition well outside the focal spot, a target of the type indicated in Figure 11 was fabricated. Here we have a linear array of surface thermocouples, each separated by 3.2 mm, the middle one of which is illuminated by the focused laser beam. For low intensity pulses, a response is observed only on TC3. When breakdown occurred, however, all five thermocouples registered responses. (Note the difference in scales.) We also see a time delay for response of the outer thermocouples, consistent with measured plasma expansion velocities. This indicates that the energy transfer to the surface is due to either conduction or very short range radiation.

To extract a coupling coefficient, the temperature histories of the individual thermocouples are first inverted by our computer procedure to find the heating rates. Each of the heating rates is then integrated in time to give absorbed fluence as a function of position. The resulting curve is then integrated spatially to give total absorbed energy.

Following this procedure, the total thermal coupling coefficients may be evaluated. In Table I these coefficients are given for copper and aluminum. These indeed show the large enhancements previously observed with spatially-unresolved calorimetric techniques.

We may thus conclude that if the laser intensity on an aluminum or copper surface is sufficient to cause breakdown, a considerable increase in thermal coupling occurs. If however, radial expansion of the plasma outside the focal spot is significant, most of this additional energy is deposited

TABLE 1

MEASURED PLASMA ENHANCEMENT OF THERMAL COUPLING

SURFACE	COUPLING COEFFICIENT		ENHANCEMENT FACTOR
	LOW INTENSITY	WITH PLASMA	
Aluminum	.039	.27	~ 7
Copper	.036	.33	~ 9

outside the focal spot, and will not greatly decrease burn-through times.

On the other hand, if the spot size is sufficiently large so that the plasma propagation is effectively one-dimensional, one would expect most of the energy to be deposited within this spot. In this case, definite fluence coupling enhancement should be observed. In the next section we report experimental results which confirm this expectation.

III. LARGE-SPOT EXPERIMENTS

The experiments were performed with one of our 500-Joule CO_2 lasers, which was fitted with a germanium out-coupled stable resonator. With this choice of cavity, a very nearly uniform beam was generated and directed with a 2-meter focal length mirror onto a thermocoupled target. The spot size at the target was adjusted by moving the focusing mirror along the optical axis. In this manner, effects with spot areas up to 19 cm^2 were observed. As in the small-spot experiments, a beam splitter, photon drag detector and $BaTiO_3$ calorimeter were used to monitor the pulse shape and energy on each shot, while plasma plumes were observed with a photomultiplier and open-shutter photography.

It is well known that repeated breakdowns on a target surface can significantly increase the breakdown threshold and decrease its strength.[3] In order to ensure a consistent plasma from pulse to pulse, the aluminum targets were cleaned with "Scotch-Brite" and wiped with methanol after each shot. This resulted in a very stable and well defined surface breakdown threshold of about 2×10^6 W/cm^2 (~ 4 J/cm^2). Repeated irradiation of the same spot without using this procedure results in a decreased thermal coupling due to

the increase in breakdown threshold. The titanium targets were in as-received condition and were irradiated only once.

Figure 12 shows a plot of thermal coupling coefficient (α) vs. incident laser fluence (E/A) for three different-sized rear-thermocoupled aluminum targets. [In this and subsequent figures, the lines through the points are merely for convenience in viewing and do not represent a fit to a theoretical curve.] The absorbed energy was determined by measuring the bulk temperature increase of the target. Spot areas of 6.3 cm^2, 12.9 cm^2 and 19.0 cm^2 were used, which in each case were approximately 12% smaller in linear dimension than the target. The coupling coefficients obtained therefore are a measure of energy deposited near the focal spot. It is seen from these curves that above breakdown threshold, there is a considerable enhancement in coupling over the low-intensity value. The coupling peaks near threshold and decreases with increasing laser fluence. Moreover as the spot size is increased, the degree of enhancement in coupling coefficient is also increased somewhat. This indicates that for large spots a slightly larger fraction of the incident energy is coupled to the target in the focal spot area.

As is shown in Figure 13, the coupling coefficients we have measured peak at comparable values to those measured by Rudder[1] at AFWL with his small (.062 cm^2) focal spot, but fall off much faster with increasing laser fluence. This results in part from the fact that for equal laser intensities, more plasma energy is dissipated radially for a very small spot than for a larger one, thus reducing the plasma density and hence the velocity at which it recedes from the surface. Therefore, at high intensities and small focal

spots the laser energy is absorbed closer to the target and is more efficiently transferred to it. It should be kept in mind, however, that for such small spots most of the energy is absorbed by the target outside the focal spot.

Another contributor to the rapid fall-off of α with E/A in our case may be the large and relatively broad initial spike associated with our cavity design (see Figure 17). Klosterman et al.[7], have observed and Jackson and Nielsen[8] have calculated that the shock associated with ignition of an absorption wave can raise its propagation velocity substantially over what it would be were the wave translating into quiescent air. This increased velocity was found to persist long after ignition. If that be the case, our strong spike, which in all cases induces the breakdown, may increase considerably the velocity at which the absorption wave recedes from the target, even after the spike is over. This would result in a more effective decoupling of the laser radiation than would be the case were there no spike.

To test the above hypothesis, we plan to perform thermal coupling experiments with the spike eliminated or greatly reduced. We have previously demonstrated that this can be done, using either saturable absorbers or electron-gun current modulation. Streak photography will be employed to determine the effect of the spike on the propagation velocity of the plasma. The upcoming thermal experiments on the AVCO Humdinger, with its less prominent spike should also shed light on this phenomenon, as well as providing large-spot data points at the high fluences required for realistic target damage.

Figure 14 shows a plot of α vs. E/A for 2" x 2" (25.8 cm^2) targets of aluminum and titanium. For both materials, the spot area was 6.3 cm^2. Also shown is the plot from Figure 13 in which the spot area was also 6.3 cm^2, but the target area was only 8.5 cm^2. We see that above breakdown threshold, the curves for aluminum and titanium are identical to within the scatter of the data, indicating that in this regime, the absorptivity is controlled by the plasma and is independent of target material. If the target is normally highly absorbing, this may in fact result in a decrease in coupling coefficient, as is the case for titanium at high incident fluence. By comparing the two curves for aluminum, we see as well that a relatively small fraction of the energy is absorbed far from the focal spot.

Coupling data were also obtained for aluminum targets as a function of ambient air pressure, and the results are plotted in Figure 15. The measured values of α at 200 torr are quite close to those at 760 torr except for the difference in breakdown threshold. The curve changes markedly, however as the pressure is reduced to 0.5 torr. Although the coupling is less than in air at low fluences, it surpasses it at about 26 J/cm^2 and peaks (at a lower value than at 760 torr) at about 40 J/cm^2. This behavior is due to diffuseness of the air plasma at this low pressure. These results imply that, as shown in Figure 16, considerably more energy per unit are can be deposited on a target at high altitude than at sea level.

In order to determine the spatial distribution of the absorbed energy, we fabricated several targets of the surface - thermocoupled type previously used to obtain our small spot data. The targets used in this study contained

a linear array of six aluminum-coated thermocouples, 1/4 inch apart, enabling us to determine the absorbed energy distribution both inside and outside the focal spot.

Figure 17 shows a comparison of the pulse shapes of the incident and absorbed intensity for a point inside the focal spot. The pulses are normalized to equal areas. It is seen that the initial spike is quite efficient in coupling energy to the surface since the plasma has not moved appreciably. As the plasma recedes, decoupling sets in. At the end of the pulse, however, an appreciable amount of energy is still being absorbed. This indicates that increasing the pulse length may increase the maximum deliverable fluences.

Figure 18 shows the absorbed fluence in air as a function of position for three different incident laser energies. These fluences were extracted from the observed temperature histories by means of our computer inversion of the one-dimensional heat equation. These curves show the spreading of the absorbed energy distribution as the laser energy is increased.

IV. CONCLUSIONS

We may summarize this work by the following conclusions.

1. Thermocoupled targets can be constructed which measure the thermal response of a metal surface with microsecond temporal resolution and 10 mil spatial resolution.

2. There is a marked enhancement in thermal coupling to aluminum and copper surfaces at the onset of breakdown. For 2 mm spots, however, most of this enhanced absorption occurs outside the focal spot.

3. Enhancement of thermal coupling is retained with large focal spots, but the coupling decreases faster with incident laser fluence than with small spots.

4. The fraction of energy coupled to the target within the focal spot increases with increasing spot size.

5. Above the target-dependent breakdown threshold, the thermal coupling is material independent.

6. For high incident fluences, more energy is transferred to the target at 0.5 torr than at 760 torr.

7. Experiments should be done to determine the effect on thermal coupling of

   a) removing or reducing the initial spike

   and

   b) increasing the pulse length

REFERENCES

1. R. R. Rudder, First DoD Conference on High Energy Laser Technology, San Diego, October 1974.

2. S. Marcus, J. E. Lowder, S. Manlief, and D. L. Mooney (to be published).

3. R. B. Hall, J. D. McClure, W. B. Maher, D. B. Nichols, and P. S. I. Wei, Boeing Aerospace Company, Interim Progress Report, Contract Number F29601-73-A-0038-6002 (February 1975).

4. C. J. Scott, "Transient Experimental Techniques for Surface Heat Flux Rates," in Measurement Techniques in Heat Transfer, edited by E. R. G. Eckert and R. J. Goldstein (CIRCA Publications, Inc., New York, 1970).

5. H. E. Fettis, Math. Comp. 18, 491 (1964).

6. H. S. Carslaw and J. C. Jaeger, Conduction of Heat in Solids (Clarendon, Oxford, 1959).

7. F. L. Klosterman, S. R. Byron, and J. F. Newton, Laser Supported Combustion Waves Study, Interim Report, Air Force Weapons Laboratory, (1973).

8. J. P. Jackson and P. E. Nielsen, Air Force Weapons Laboratory, Laser Digest, AFWL-TR-74-100, 212 (1974).

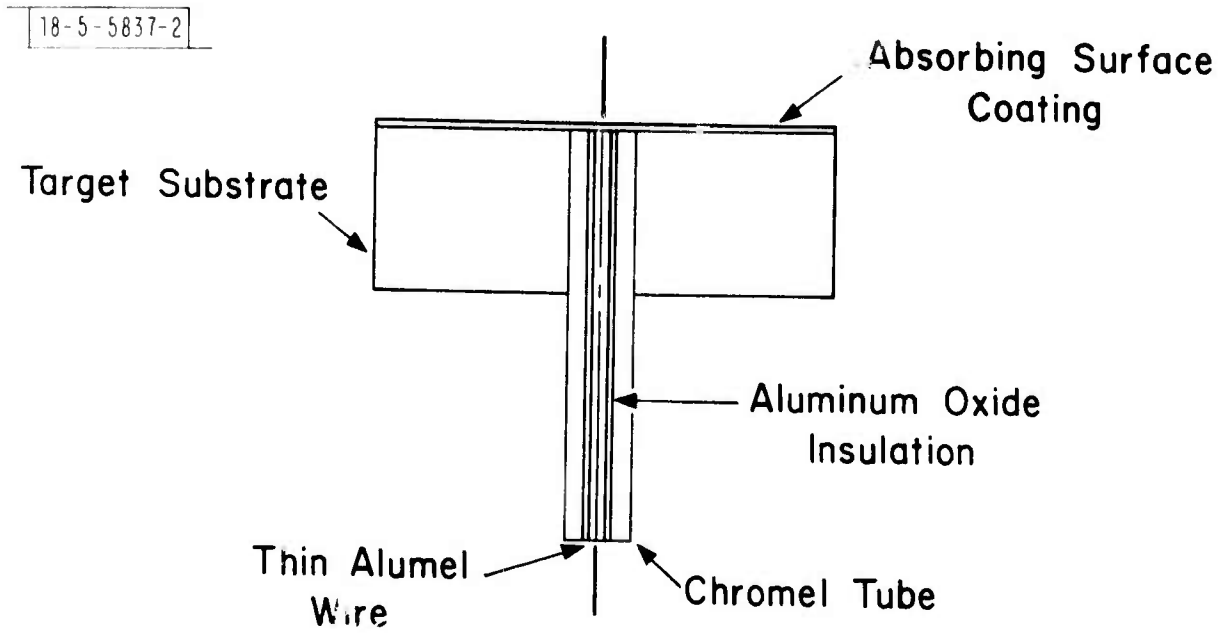

Fig. 1. Surface-thermocoupled target structure.

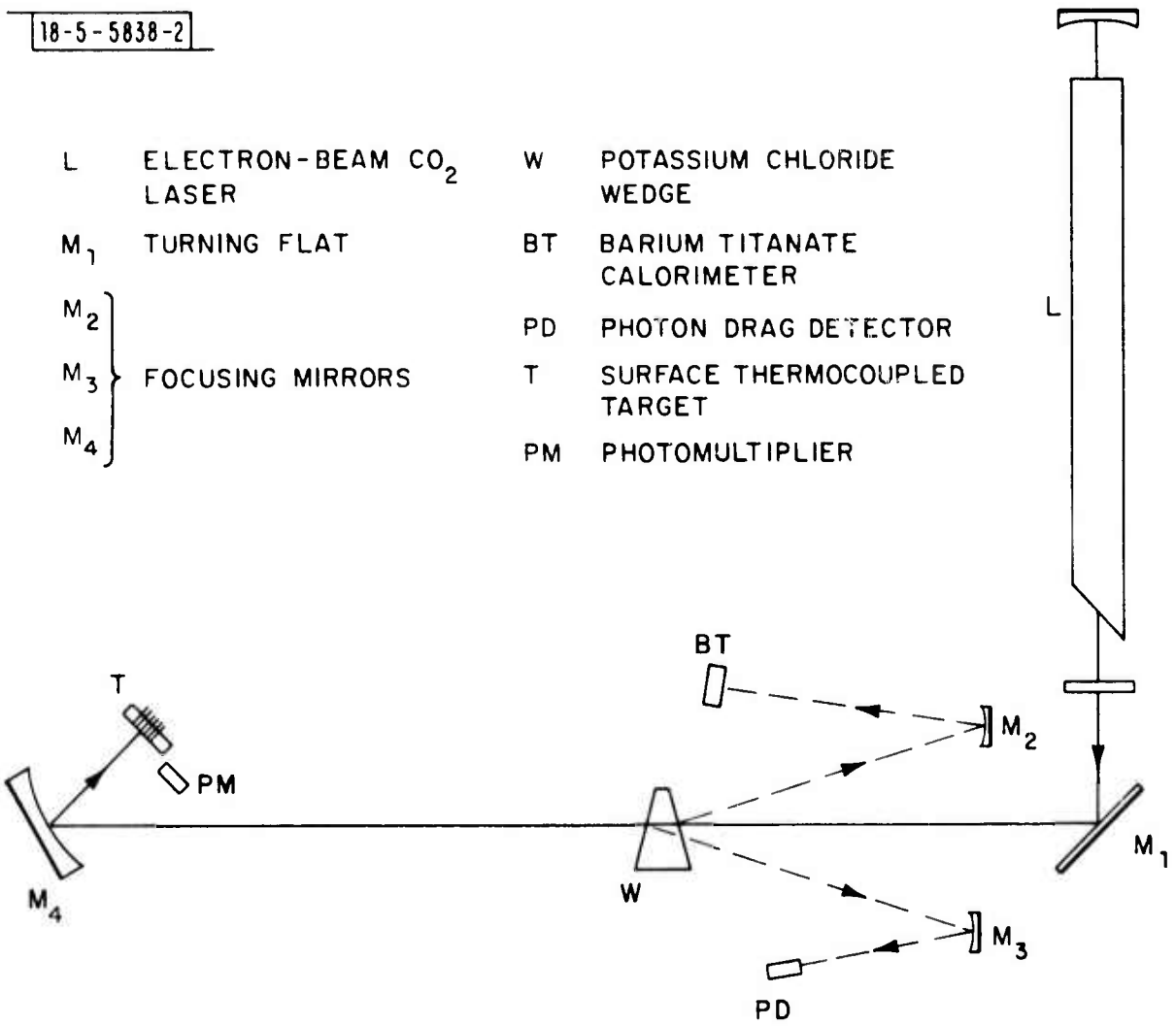

Fig. 2. Experimental layout for thermal-coupling measurements.

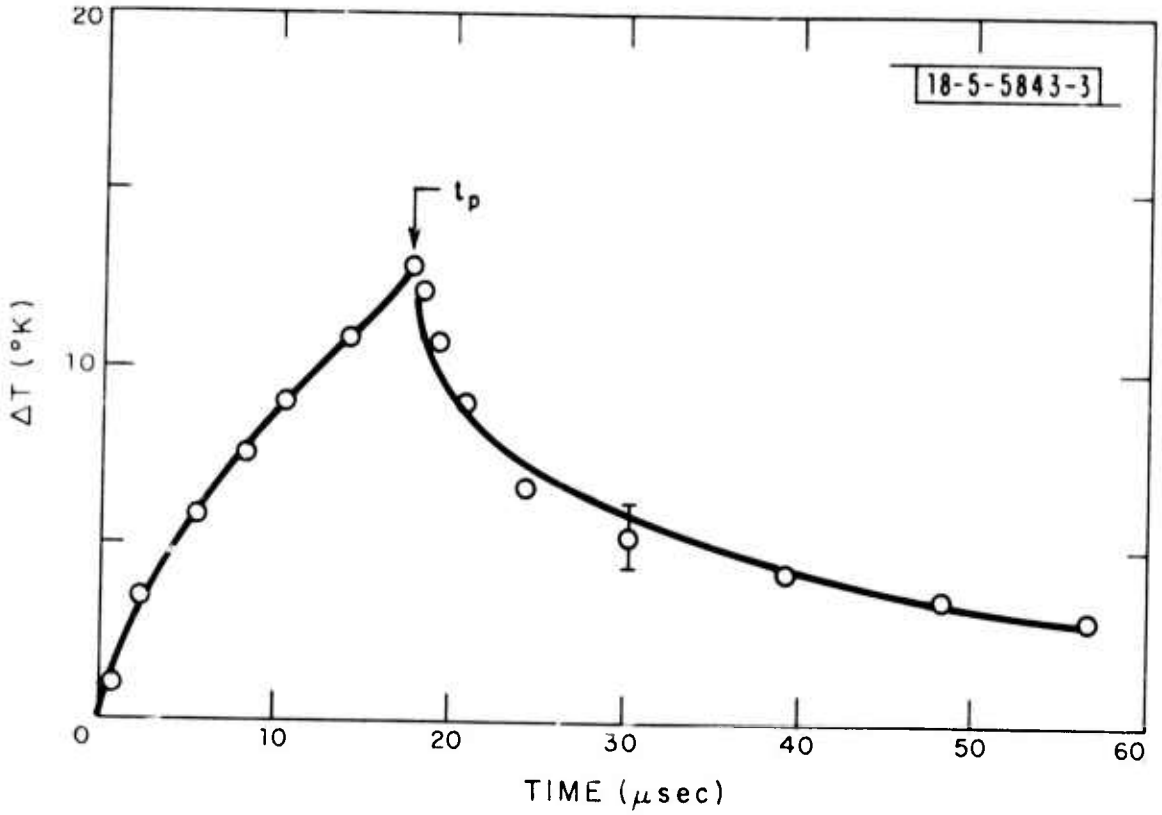

Fig. 3. Surface temperature history for copper surface; average incident power density of 8.3×10^4 W/cm^2 with no visible surface plasma.

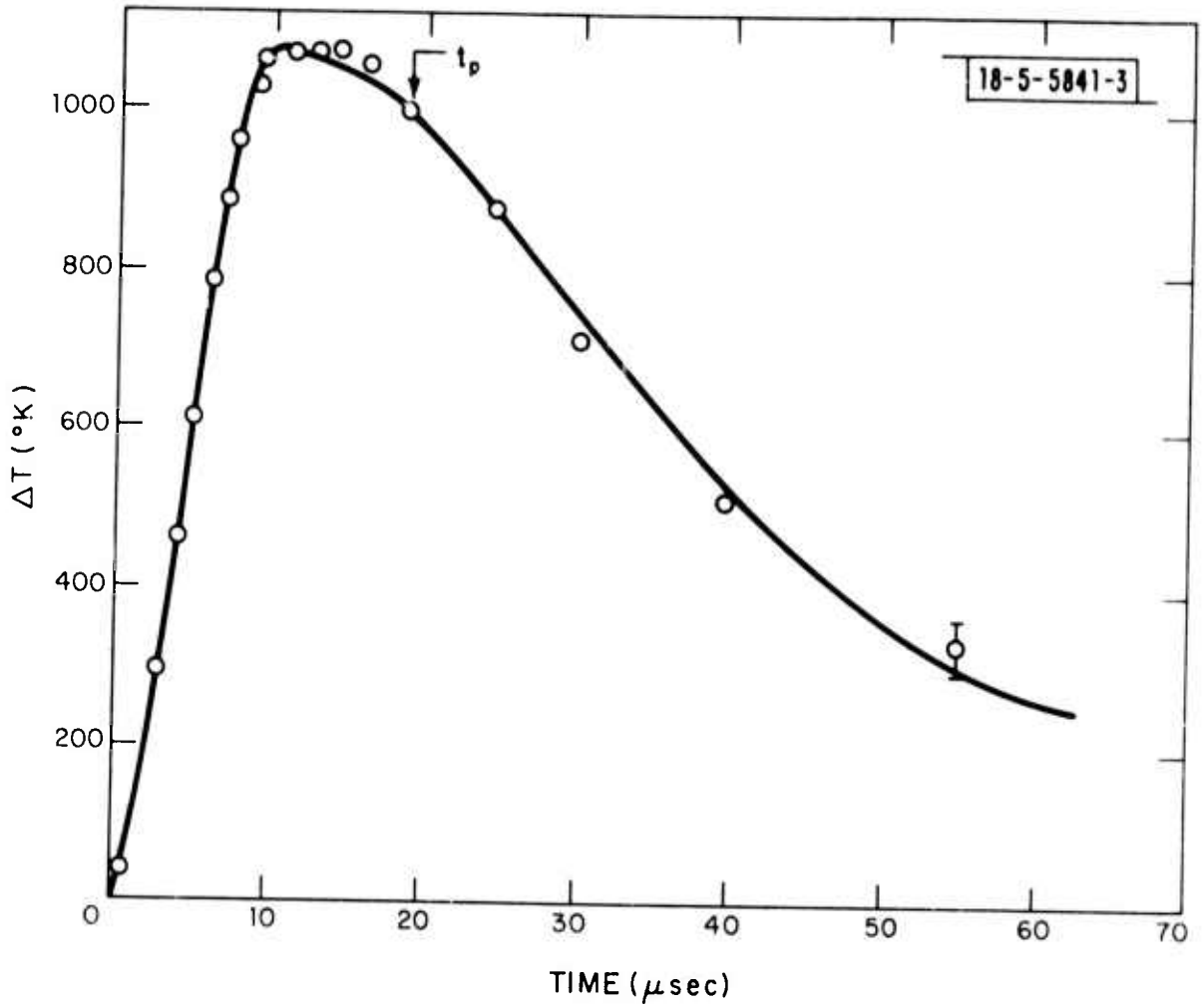

Fig. 4. Surface temperature history for copper surface; average incident power density of 5×10^6 W/cm^2 with a strong surface plasma initiated immediately.

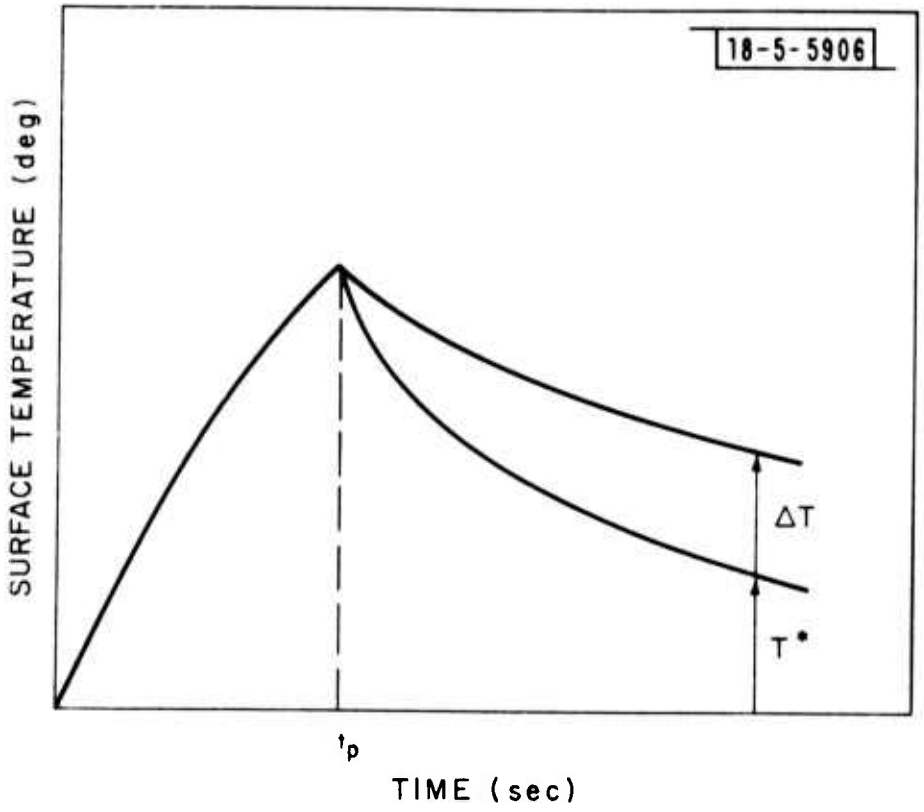

Fig. 5. Illustration of the temperature (T*) due to heating prior to time t_p and the contribution ΔT due to heating after time t_p.

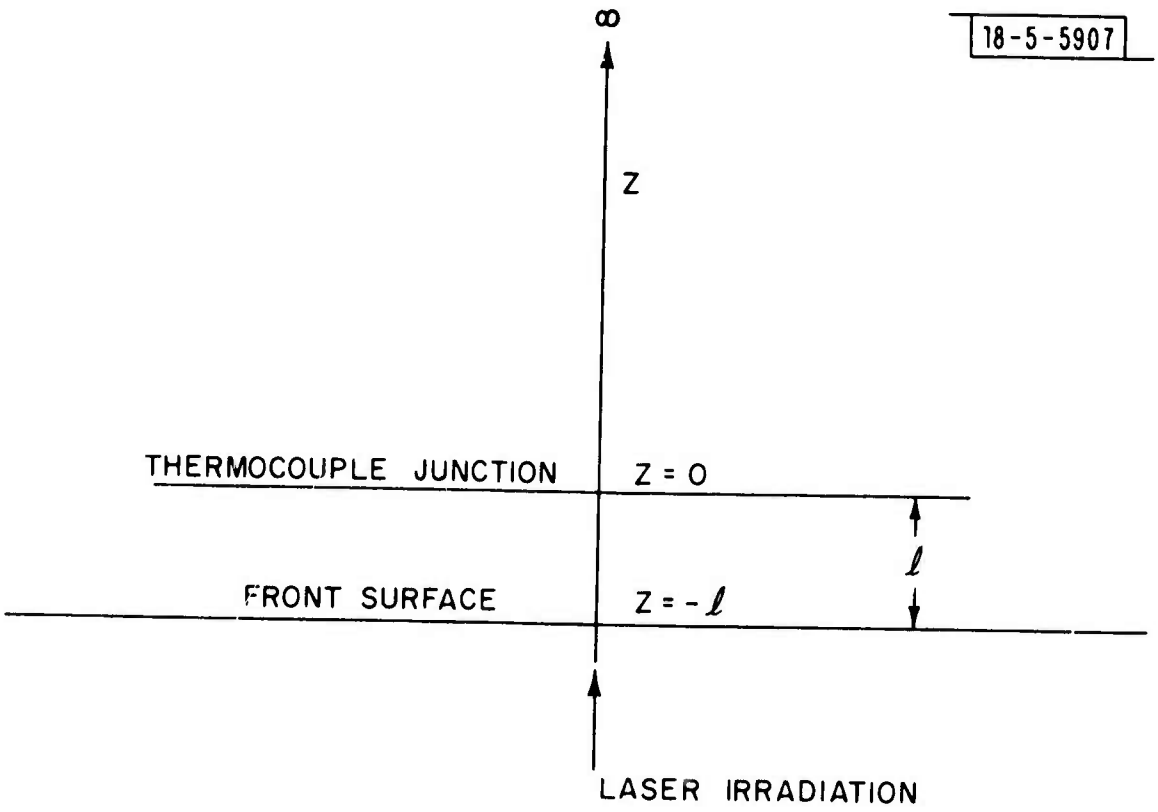

Fig. 6. Coordinate system for subsurface thermocouple junctions.

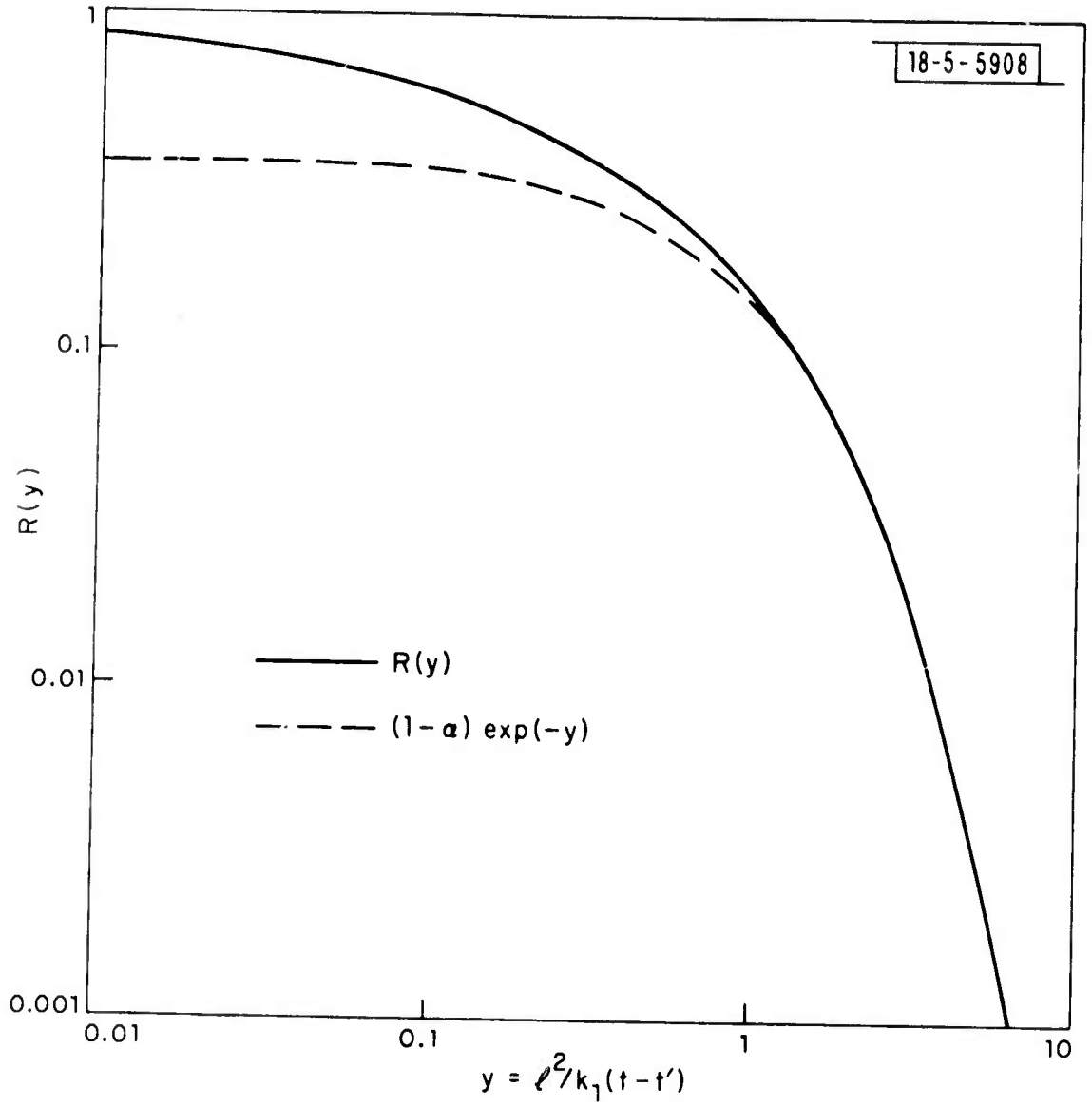

Fig. 7. The "depth function" R(y) for subsurface thermocouple junctions.

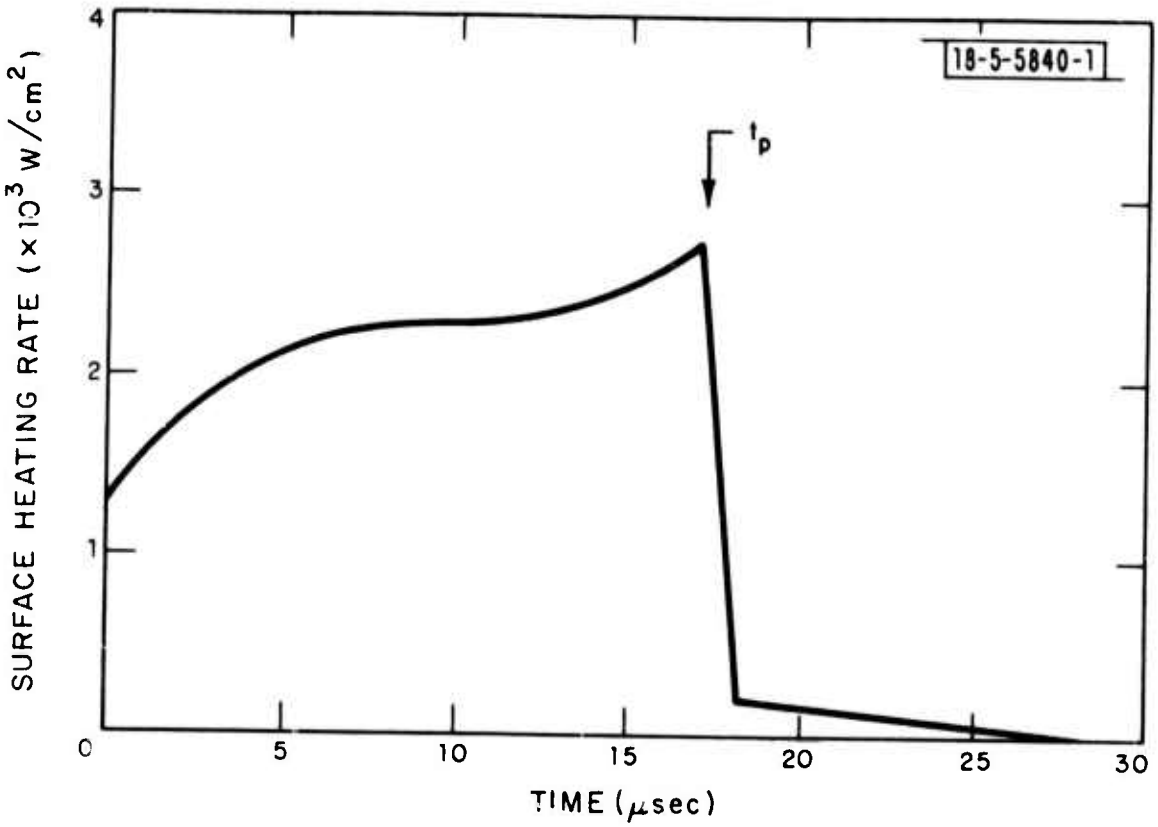

Fig. 8. Surface heating rate determined from inversion of surface temperature history shown in Fig. 3; average absorption coefficient was 2.7 percent.

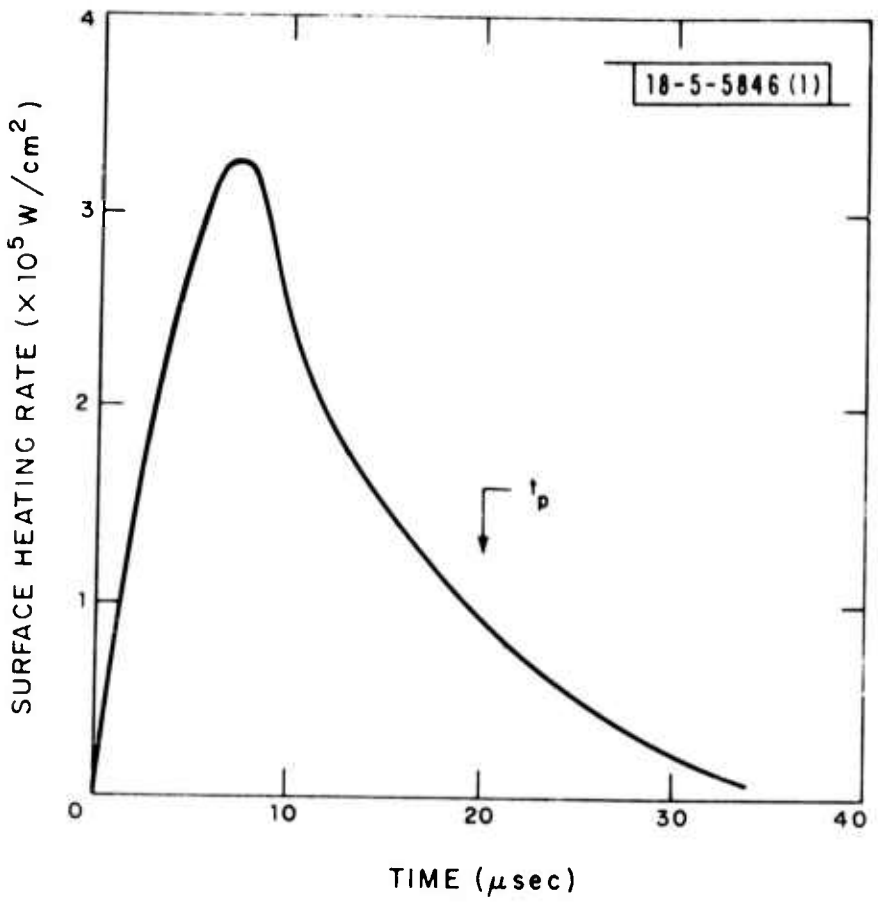

Fig. 9. Surface heating rate determined from inversion of surface temperature history shown in Fig. 4; average absorption coefficient was 4.2 percent.

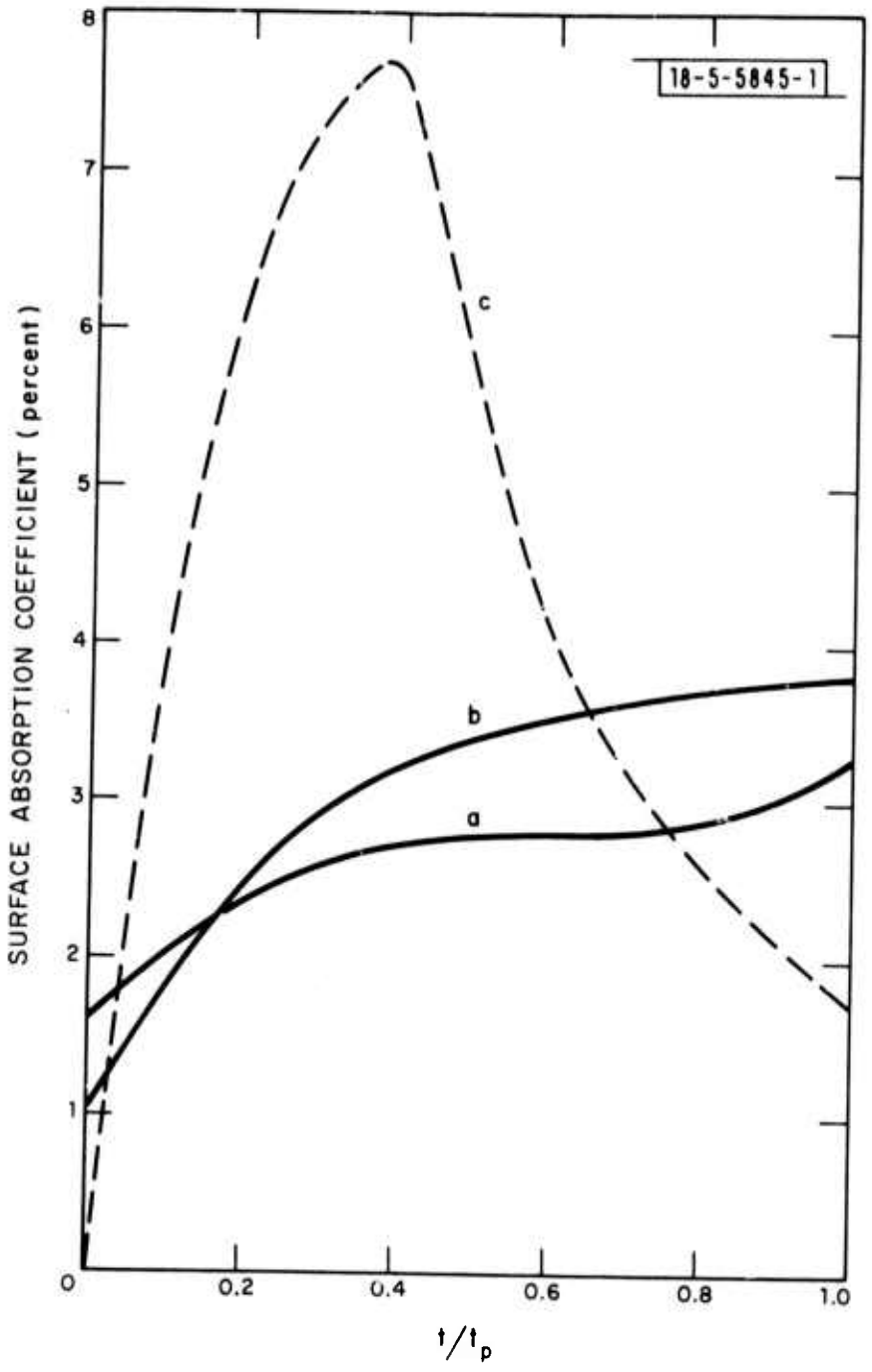

Fig. 10. Surface absorption coefficients as functions of time normalized by the pulse lengths for (a) no surface plasma ($I \sim .08$ MW/cm^2, $t_p = 18$ μsec - see Fig. 8); (b) near breakdown threshold ($I \sim 0.3$ MW/cm^2, $t_p = 32$ μsec); (c) strong surface plasma ($I \sim 5$ MW/cm^2, $t_p = 20$ μsec - see Fig. 9).

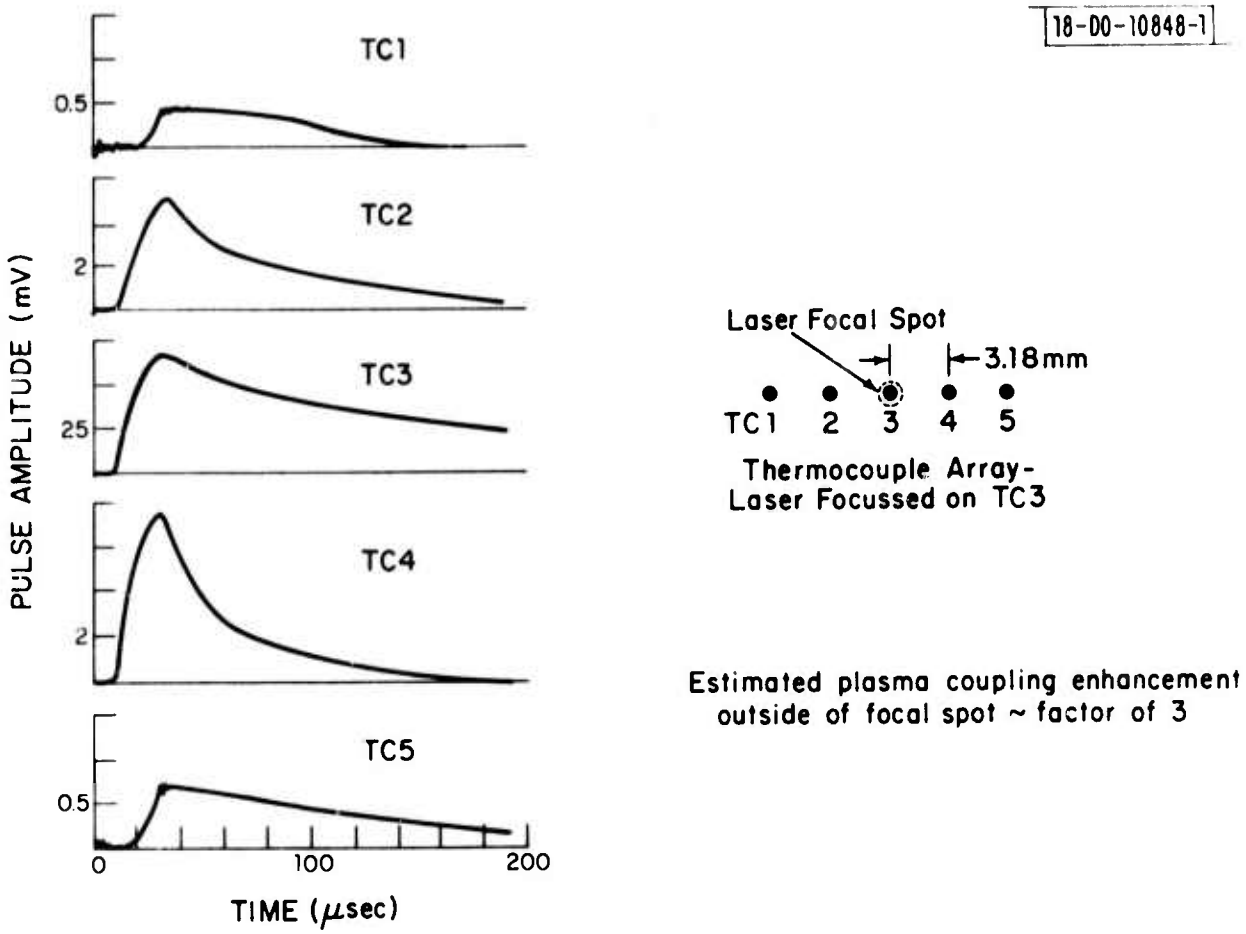

Fig. 11. Thermocouple traces for the case of breakdown on a copper target containing the linear array of surface thermocouples shown schematically.

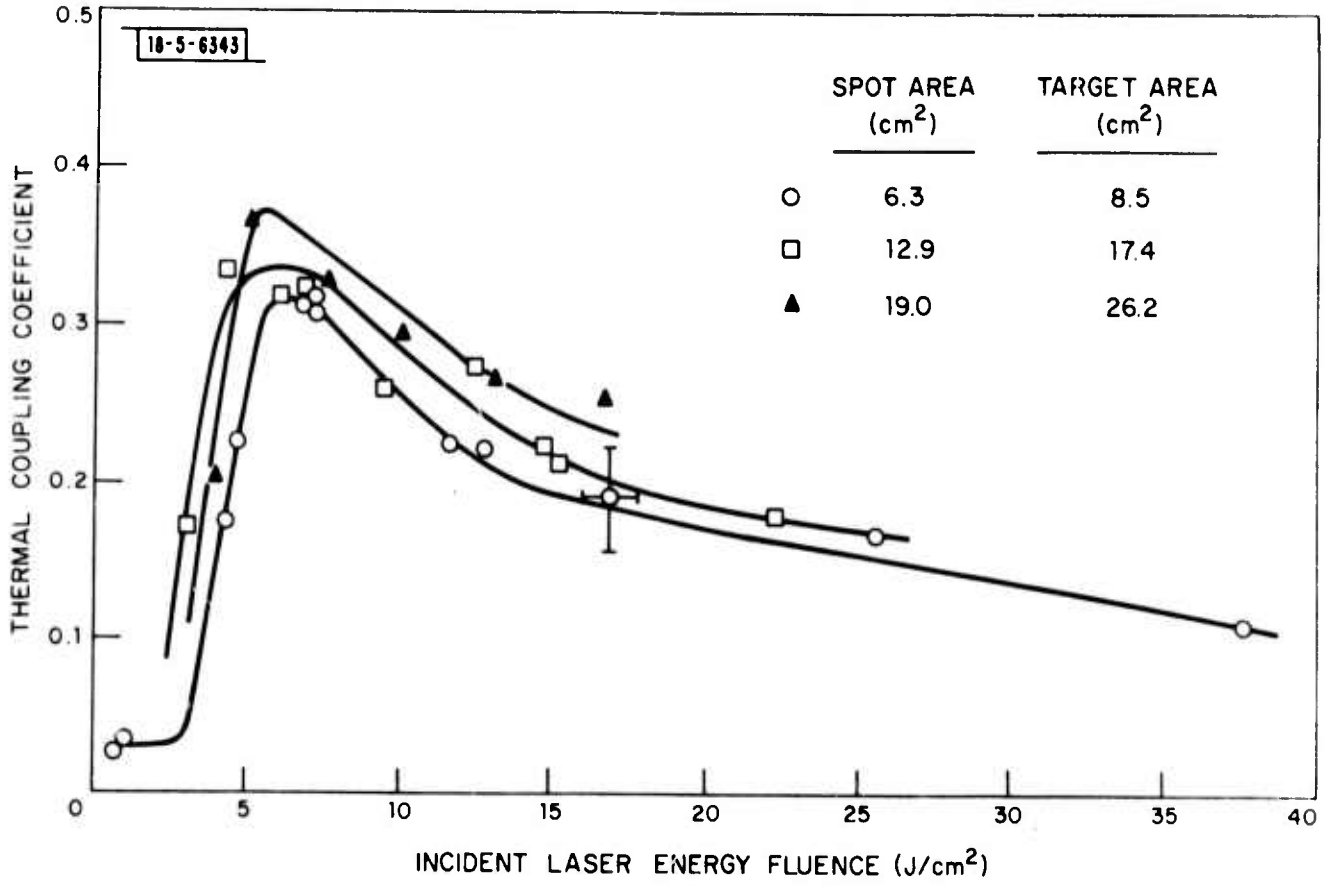

Fig. 12. Spot size dependence of thermal coupling to an aluminum target, the typical error is shown for one point.

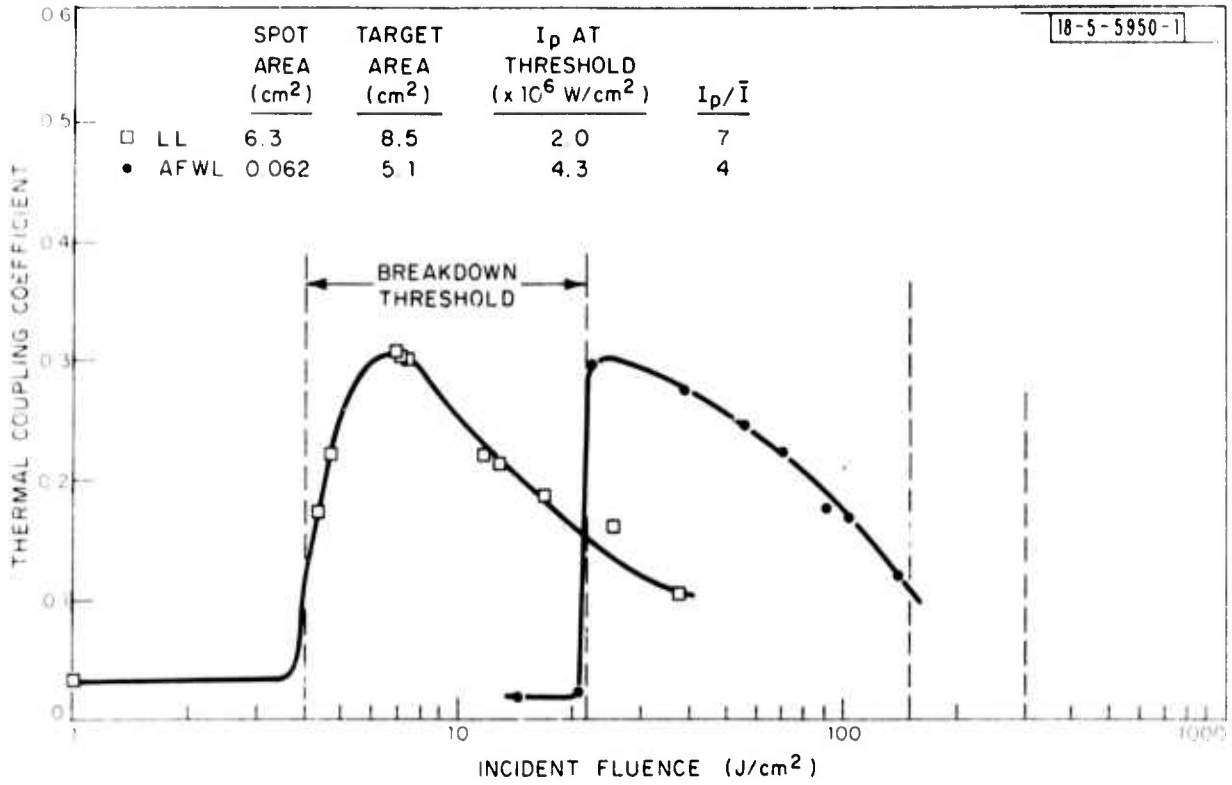

Fig. 13. Pulsed thermal coupling to aluminum at 10.6 μm

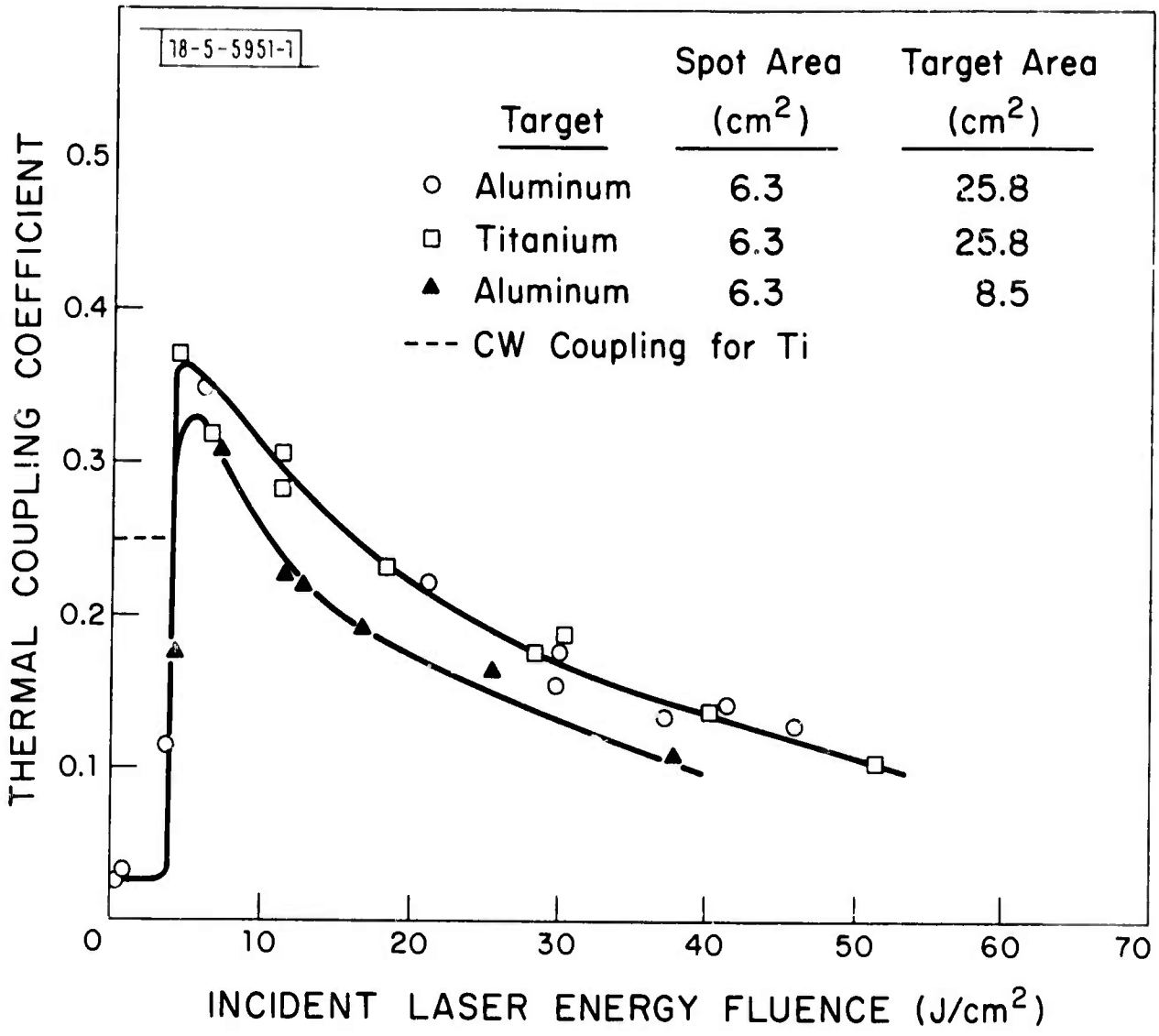

Fig. 14. Material and target-size dependence of thermal coupling.

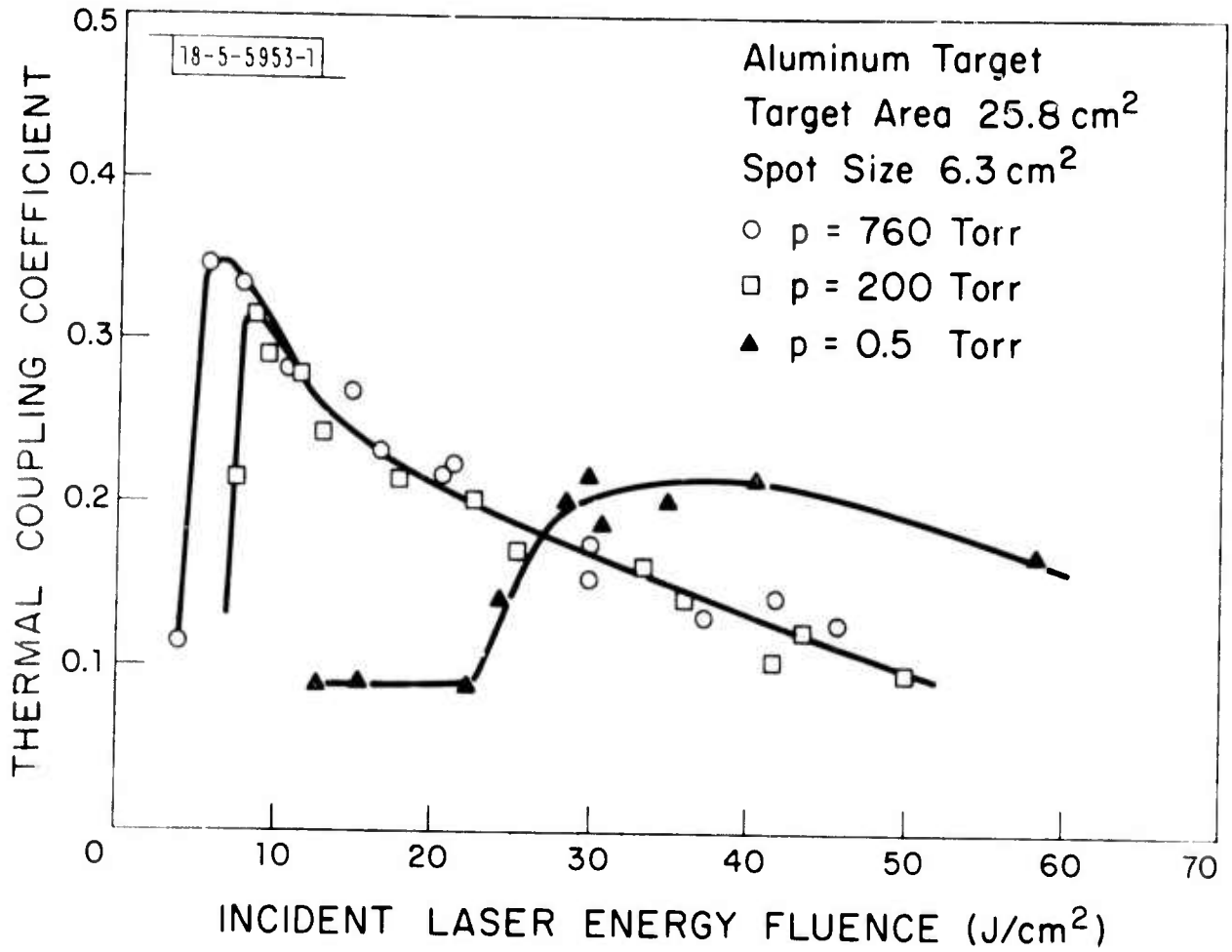

Fig. 15. Pressure dependence of thermal coupling.

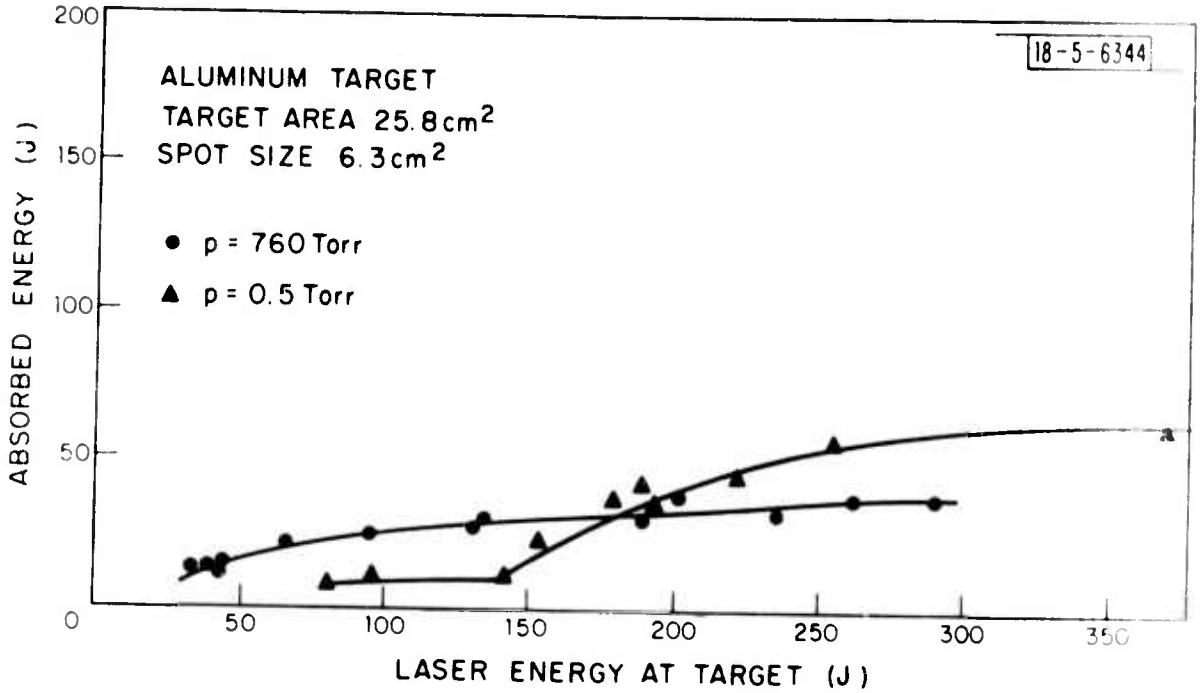

Fig. 16. Pressure dependence of absorbed energy.

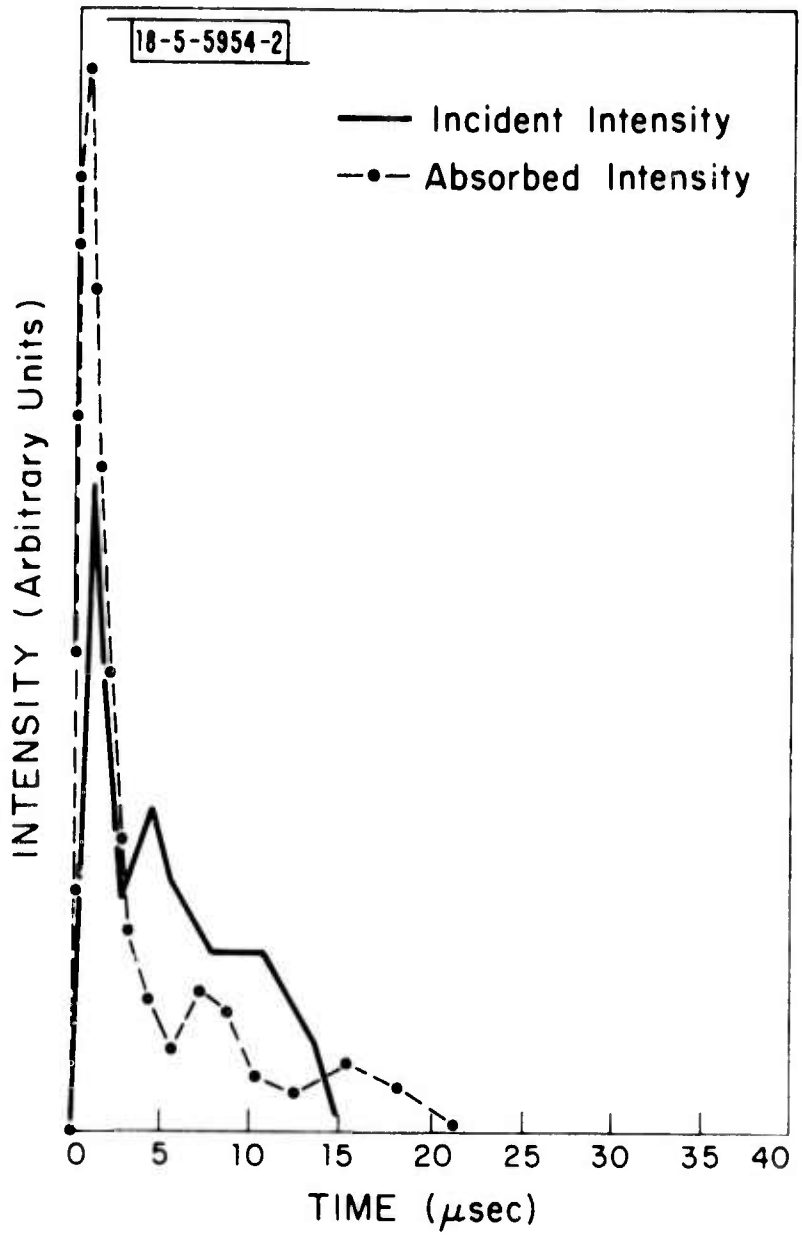

Fig. 17. Pulse shapes of incident and absorbed intensity.

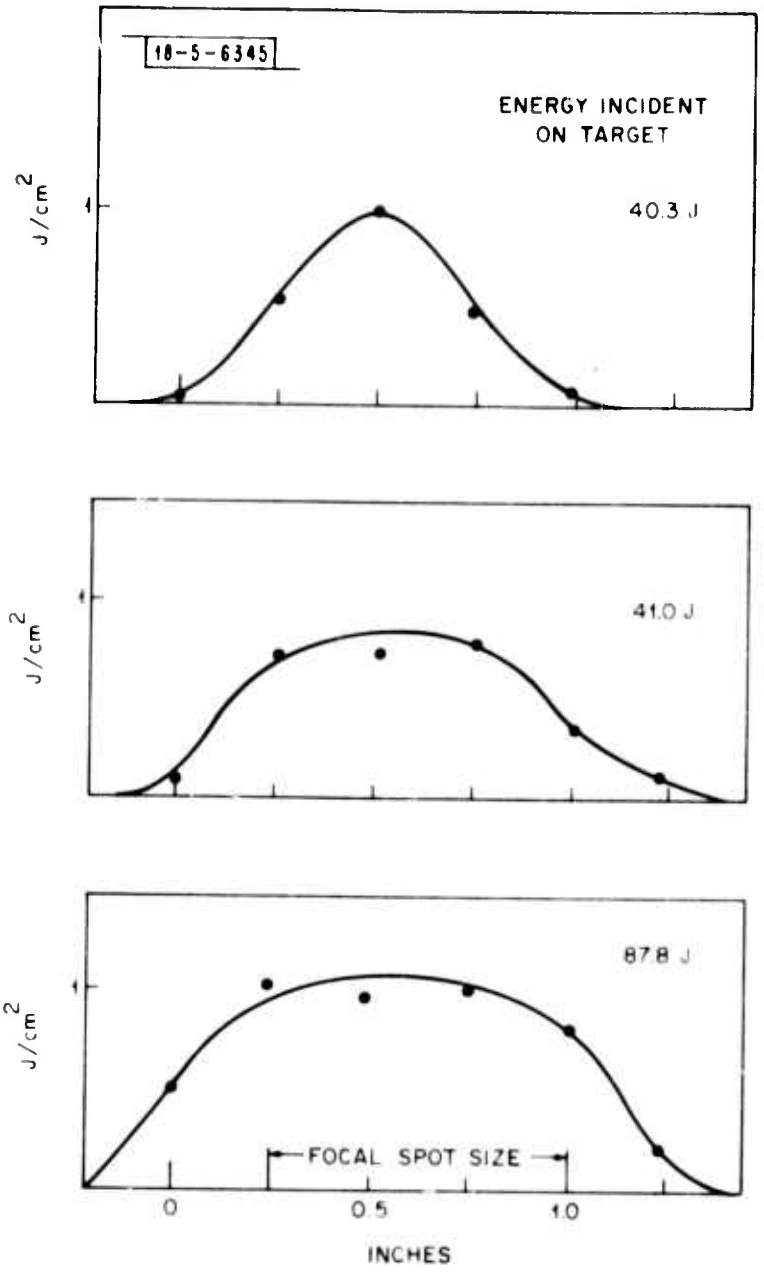

Fig. 18. Spatial distribution of absorbed energy for three different incident laser energies.